(Volume: 230 Issue: 1) pp.30-38. Copyright ©2015 SAGE Publications. DOI: 10.1177/0954411915616987.

Individual and combined effects of noise-like whole body vibration and parathyroid hormone treatment on bone defect repair in ovariectomized mice

Takeshi Matsumoto[1,3], Daisuke Sato[2], and Yoshihiro Hashimoto[3]

[1]Department of Mechanical Engineering, Tokushima University Graduate School of Advanced Technology and Science, Tokushima, Japan

[2]Department of Systems Science, Osaka University School of Engineering Science, Toyonaka, Japan

[3]Department of Mechanical Science and Bioengineering, Osaka University Graduate School of Engineering Science, Toyonaka Japan

Corresponding author:

Takeshi Matsumoto, Department of Mechanical Engineering, Tokushima University Graduate School of Advanced Technology and Science, 2-1 Minamijyousanjima-cho, Tokushima 770-8506, Japan

Email: t.matsumoto@tokushima-u.ac.jp

Abstract

The effectiveness of intermittent administration of parathyroid hormone (iPTH) and exposure to whole body vibration (WBV) on osteoporotic fracture healing has been previously investigated, but data on their concurrent use are lacking. Thus, we evaluated the effects of iPTH, WBV, and their combination on bone repair in osteoporotic mice. Noise-like WBV with a broad frequency range was used instead of conventional sine-wave WBV at a specific frequency. Mice were ovariectomized at 9 weeks of age, and subjected to drill-hole surgery in the right tibial diaphysis at 11 weeks. The animals were divided into four groups (n=12 each): a control group (C), and groups treated with iPTH (P), noise-like WBV (W), and both (PW). From postoperative day 2, the P and PW groups were subcutaneously administered PTH at a dose of 30 μg/kg/day. The W and PW groups were exposed to noise-like WBV at a root mean squared acceleration of 0.3 g and frequency components of 45 to 100 Hz for 20 min/day. Following 18 days of interventions, the right tibiae were harvested, and the regenerated bone was analyzed by micro-computed tomography and nanoindentation testing. Compared with C, callus volume fraction was 40% higher in P and 73% higher in PW and callus thickness was 35% wider in PW. Indentation modulus was 46% higher in W and 43% higher in PW, and hardness was 31% higher in PW compared with C. There was no interaction between the two treatments for both structure and mechanical indexes. The main effects of iPTH and noise-like WBV on bone repair included increased bone formation and enhanced mechanical function of regenerated bone, respectively. The combined treatment resulted in further regeneration of bone with high indentation modulus and hardness, suggesting the therapeutic potential of the combined use of noise-like WBV and iPTH for enhancing osteoporotic bone healing.

Keywords

Osteoporotic bone repair, noise-like vibration, parathyroid hormone, micro-computed tomography, nanoindentation testing

Introduction

As a corollary of the aging global population, osteoporosis has become an important healthcare issue for the elderly. Osteoporosis is characterized by low bone density and microarchitectural deterioration of bone tissue. Because of low peak bone mass coupled with menopausal bone loss, osteoporosis is more prevalent in postmenopausal women.[1] More than 200 million postmenopausal women worldwide suffer from osteoporosis. According to the X-ray analysis of the lumbar spine and femoral neck in a large-scale population-based cohort study,[2,3] there are 9.8 million women and 3 million men aged 40 years and over currently suffering from osteoporosis in Japan. Osteoporosis increases bone fragility and susceptibility to fracture,[4] resulting in increased morbidity and mortality, as well as decreased functionality and quality of life. Although more attention has been paid to fracture prevention than healing, the prevention and treatment of osteoporosis-induced fractures in older patients have both economic and health benefits.

The healing process of osteoporotic fractures is often impaired. Rodent models of postmenopausal osteoporosis following ovariectomy (OVX) have been widely used to show impaired fracture healing.[5-10] Although OVX models are of limited value in reproducing postmenopausal osteoporosis[11] and impairment of fracture healing in osteoporosis remains to be clarified,[12,13] it is of clinical importance to enhance its healing to allow for early rehabilitation of patients and restoration of adequate functionality. A number of studies have focused on the effects of pharmacological treatments for osteoporotic fracture healing in OVX animals.[14-16] Among these treatments, parathyroid hormone (PTH), the first bone anabolic drug approved for the treatment of osteoporosis, was shown to be effective in reducing OVX-induced impairment of fracture healing. Intermittent PTH (iPTH; i.e., once-daily administration of PTH) causes an anabolic response and enhances fracture healing of OVX rats.[17-20] Beneficial effects of iPTH on fracture healing in postmenopausal women have also been reported.[22,22] Furthermore, several studies demonstrated the enhancement of the anabolic effect of iPTH in combination with mechanical loading[23-28] and its reduction by unloading[29,30] in intact rodent bone. It was also reported

that the combined treatment of iPTH and mechanical loading had synergistic anabolic effects on fracture healing.[31]

Whole body vibration (WBV), which exposes subjects to low-intensity high-frequency mechanical stimuli,[32,33] has been studied for its effect in promoting fracture healing in OVX rodents.[34-39] It is anticipated that the concurrent use of WBV and iPTH could be effective in promoting fracture healing, but data are lacking. In this study, we exposed OVX mice with a tibial bone defect to WBV, and examined its pro-osteogenic effect when used singly and concurrently with iPTH. Sine-wave WBV has been exclusively used in earlier studies, but the effective frequency of WBV for enhancing fracture healing varied among studies. Thus, we used noise-like WBV with a broad frequency range to reduce the likelihood of ineffective WBV at a specific frequency. Micro-computed tomography (μCT) and nanoindentation testing were performed to evaluate structure and intrinsic mechanical properties of regenerated bone, respectively.

Method and Materials

General Procedures

Experiments were conducted in accordance with the guiding principles of the American Physiological Society and with the approval of the Animal Research Committee of Osaka University Graduate School of Engineering Science. Female C57BL/6 mice (Clea Japan, Tokyo, Japan), an inbred strain exhibiting highly mechanosensitive bones,[40,41] were bilaterally ovariectomized under anesthesia by intraperitoneal injection of ketamine (100 mg/kg) and xylazine (10 mg/kg) at 9 weeks. Mice were then single-housed in a plastic cage under controlled conditions (12-hour light/dark cycle, 25°C, 60% humidity), and allowed free access to a standard diet (CE-2; Clea Japan) and tap water. Two weeks later, all mice were anesthetized with intraperitoneal pentobarbital sodium (50 mg/kg). The skin over the medial aspect of the right lower leg was shaved, swabbed with povidone iodine, and incised. A full-thickness unicortical hole was created

approximately 3 mm proximal to the tibio-fibula junction using a 0.5-mm diameter drill rotating at 11, 000 rpm (Muromachi Kikai, Kyoto, Japan). Drill margins were frequently irrigated with saline to avoid thermal necrosis, and the drill hole was rinsed with a flushing syringe to discard bone fragments. After the arrest of bleeding from the bone marrow, the skin was sutured and swabbed again.

Mice were randomly divided into four groups (n=12 each): the control group (C), and groups treated with iPTH (P), noise-like WBV (W), and both (PW). The P and PW groups were subcutaneously administered recombinant human PTH (1–34) (Bachem California, Inc., Torrance, CA), dissolved in a vehicle of 0.2% bovine serum albumin and 0.1% 1 mN hydrochloric acid in 0.9% saline to form a solution of 10 μg/ml for delivery,[42] at a dose of 30 μg/kg/day. The C and W groups received only the delivery vehicle at an equal volume as in the P and PW groups. Additionally, mice in the W and PW groups were exposed to noise-like WBV at a root mean squared acceleration of 0.3 g and frequency components from 45 to 100 Hz (Gaussian quasi-white noise) for 20 min/day. This frequency range included vibration regimes with reported efficacy for bone formation in OVX rodents.[36,39,43,44] Six mice at a time were placed in a compartmented cage fixed on a rigid platform vibrating vertically in a noise-like manner (Fig. 1A). Mice in the C and P groups were placed on the vibration platform for 20 min/day but in a non-operating state. The vehicle or PTH was administered 30 min before each WBV session.

The interventions were commenced on the second day following drill-hole surgery and introduced daily thereafter at the same time. After 18 days of treatment, mice were euthanized by an overdose of pentobarbital sodium. The drill-holed tibiae were harvested, dissected free of soft tissue, wrapped with moistened saline gauze and stored at −30°C until analysis.

Vibration generator

The platform was driven by an electromagnetic actuator (SW-2015; Asahi Seisakusyo, Tokyo, Japan), connected to a power supply/amplifier (APD-200FCA; Asahi Seisakusyo) and a vibration controller (K2

Sprint; IMV, Osaka, Japan). Data on a target acceleration waveform and frequency characteristics of the platform were loaded to the vibration controller via a software interface on a Windows PC. The target waveform was produced by band-pass filtering a zero-centered 20-min Gaussian quasi-white noise signal between 45 and 100 Hz and scaled to yield the root mean squared acceleration of 0.3 g. The Gaussian white noise signal was generated using a computer freeware package (Wavegene ver. 1.50, Japan). The frequency characteristics of the platform integrated with the cage, including lead weights as substitutes for mice, were acquired using data received from an accelerometer (P51SC; Fuji Ceramics, Tokyo, Japan) mounted on the cage. Following a finite-length waveform control procedure based on the feed-forward method, the vibration controller generated the input signal, which controlled the gain of the amplifier to produce the required actuator vibration. Part of the actual vibration measured at the cage bottom using the accelerometer and a laser displacement sensor (LK-H052/G5000V; Keyence, Osaka, Japan) is shown in the time domain (acceleration and displacement waveforms) and frequency domain (acceleration spectrum) in Fig. 1B.

μCT Analysis

The specimens were slowly thawed and encapsulated in an acrylic tube filled with saline. Then, the cortical defect site was scanned using a μCT system (SMX-1000/VCT; Shimadzu, Kyoto, Japan). For structural analysis, a cylindrical region of interest was chosen within the cortical defect (Fig. 2). Its diameter and height were set at 480 μm and 150–160 μm, respectively; the latter was close to but below the thickness of a nearby intact cortical bone region. The scanning parameters were as follows: 90 keV, 110 μA, 600-ms integration time, and 1,200 projections on 360°. The defect images were reconstructed with 9-μm voxel resolution and 8-bit gray-scale resolution. Pure bone was separated from the background by binarization using Otsu's method.[45] The following structural indexes were determined for newly formed bone: fraction of volume (Vf, %), mean thickness (Th, μm), segment number (Seg.N, mm^{-3}), and

segment connectivity density (Seg.C, mm^{-3}). The BoneJ plugin 1.3.5 for ImageJ 1.46k[46] was used to determine all indexes.

Nanoindentation testing

After μCT, the defect segment cut out from each tibiae with a low-speed diamond wheel saw (SBT650; South Bay Technology, San Clemente, CA, USA) was embedded in ambient-cured dental polymethylmethacrylate (Toughron Rebase; Miki Chemical Products Co, Kyoto, Japan) without ethanol dehydration/fixation to avoid possible deterioration of the collagen.[47] After polymerization in a water bath, using a 600-grit SiC abrasive paper disc, the proximal surface of an embedded specimen was sanded perpendicularly to the tibial long axis in deionized water until the midsection of the defect was reached. After further polishing sequentially with 1200- and 4000-grit SiC abrasive paper discs and 1-μm diamond suspension (DP-Spray P; Struers, Ballerup, Denmark), the surface was finally polished with 0.05-μm alumina suspension (AP-D; Struers, Ballerup, Denmark) to a state close to a mirror surface (Fig. 3A). The proximal cross section was ultrasonically cleaned to remove surface debris and heated at 50°C for 24 h in ambient air to prevent enzymatic degradation of collagen.[47]

Each specimen was subjected to nanoindentation testing. Indents were laid out in 2 × 10 grids in each periosteal and endosteal regenerated bone region with 30 μm spacing. Those indents falling on where bone is not yet formed or edges of newly formed bone were excluded from the analysis, resulting in 12 to 30 testing points on the regenerated bone region in each specimen, depending on its extent. A dynamic ultra-micro-hardness tester (DUH-201S; Shimadzu, Kyoto, Japan) equipped with a diamond Berkovich tip (tip curvature radius < 100 nm) was used to acquire a trapezoidal loading waveform (loading–holding–unloading),[48] from which mechanical indexes were calculated according to the method described by Oliver and Pharr.[49] A maximum load, a loading/unloading rate, and a holding period at the maximum load were set to 6.0 mN, 0.3 mN/s, and 100 s, respectively (Fig. 3B). The indentation modulus,

in combination with the local elastic modulus E_{specimen} and the Poisson ratio v_{specimen} of the specimen, is given by the following formula:

$$\text{indentation modulus} = \frac{E_{\text{specimen}}}{1 - \nu_{\text{specimen}}^2} = \left(\frac{1}{E_{\text{r}}} - \frac{1 - \nu_{\text{tip}}^2}{E_{\text{tip}}}\right)^{-1}, \qquad (1)$$

where E_{tip} (1131 GPa) and v_{tip} (0.07) are the elastic modulus and Poisson ratio of the diamond indenter, respectively, and E_{r} is the reduced modulus. The latter was derived from the slope S at the point of initial unloading ($h = h_{\text{max}}$) and the contact area A_{c}, which have a direct relationship with E_{r}:

$$\text{S} = S(h_{\text{max}}) = \left.\frac{dP}{dh}\right|_{h=h_{\text{max}}} = \frac{2}{\sqrt{\pi}} E_{\text{r}}\sqrt{A_{\text{c}}} \qquad (2)$$

The ratio of maximum force P_{max} (P at $h = h_{\text{max}}$) to A_c gives hardness, which is interpreted as a measure of strength, specifically resistance to nonelastic deformation under pressure:

$$\text{hardness} = \frac{P_{\text{max}}}{A_{\text{c}}} \qquad (3)$$

Statistics

Data are mean±standard deviation. Mechanical indexes were averaged over measurement points in each periosteal and endosteal region, as well as in the whole region, of each cortical defect. One-way analysys of variance (ANOVA) with Tukey's post-hoc test and two-way ANOVA were performed to analyze difference between groups and the potential interaction between iPTH and noise-like WBV, respectively. Mechanical indexes were compared between periosteal and endosteal regions using a paired *t*-test. Bartlett's test or an *F*-test showed no statistical difference in variances between groups for all data sets. All data were analyzed by Prism 6 (GraphPad Software; San Diego, CA), and a value of $P < 0.05$ was considered statistically significant.

Results

Body weights in C, P, W, and PW groups were 22.4 ± 0.8, 22.8 ± 0.6, 22.6 ± 0.7, and 23.2 ± 0.8 g, respectively, on the first day of interventions, and 22.7 ± 1.1, 22.9 ± 0.8, 22.4 ± 0.5, and 23.3 ± 0.8 g, respectively, on the last day of interventions. Body weight did not change significantly over time or between groups.

Figure 4 shows three-dimensional displays of regenerated bone in cylindrical regions extracted from cortical bone defects in the C, P, W, and PW groups. Regenerated bone preferentially filled the defect in the periosteal side in every group, showing increased bone formation in the periosteal region compared with the endosteal region. The spicules of woven bone in the P and PW groups extended further towards the medullary cavity than in the C group. The structural indexes of regenerated bone in the defect are summarized in Table 1. No significant difference was found in any of the structural indexes between the C and W groups. In contrast, Vf and Th were higher in the P and PW groups than in the C group. There was no significant interaction between iPTH and noise-like WBV for any structural index.

The mechanical indexes of regenerated bone are shown in Fig. 5. The number of indentation points placed in the periosteal and endosteal regions were 13.5 ± 1.9 and 6.2 ± 3.7 in the C group, 14.5 ± 1.0 and 8.5 ± 3.7 in the P group, 14.0 ± 2.0 and 8.8 ± 4.8 in the W group, and 15.0 ± 0.0 and 12.5 ± 2.4 in the PW group, respectively. For the whole defect region, no difference was found in either index between the C and P groups, but, in comparison to the C group, the indentation modulus was 46% higher in the W group and 43% higher in the PW group, while hardness was 31% higher in the PW group. Similar between-group differences were observed in the indentation modulus in each periosteal and endosteal region. Hardness did not differ between groups in either periosteal or endosteal region, but the endosteal region showed increased hardness compared with the periosteal region in the PW group. No significant interaction was found between iPTH and noise-like WBV for both mechanical indexes.

Discussion

In the present study, we showed the effectiveness of iPTH, noise-like WBV and their combination in the promotion of bone defect repair in OVX mice. Individual applications of iPTH and noise-like WBV were beneficial, particularly in increasing bone formation and enhancing the mechanical function of the bone, respectively, and the combined treatment of iPTH and noise-like WBV showed an additive effect.

A drill-hole bone defect model provides the defect site with mechanical stability. Therefore, bone arises *de novo* (intramembranous ossification) without the need for a preexisting cartilage framework (endochondral ossification).[5,50,51] Thus, although iPTH and WBV may enhance bone healing through both endochondral and intramembranous ossification,[35,37] the present result of increased bone repair by iPTH and noise-like WBV is likely due to their actions on intramembranous ossification, involving hard callus (bone) formation and remodeling.

It has been reported that iPTH is effective in recovering bone mass and increased mechanical strength in OVX animals.[52-54] The present study showed increased bone formation in iPTH-treated mice. Another study using the same dose of iPTH for a similar drill-hole defect model also demonstrated enhanced bone regeneration without endochondral bone formation.[55] However, iPTH did not affect intrinsic mechanical properties (i.e., indentation modulus and hardness) of regenerated bone, implying that iPTH is more effective in increasing the amount of callus formation than in promoting callus mineralization and remodeling.

Given that estrogen can act as a negative modulator of the mechano-sensitivity of bone cells, and that a lack of estrogen sensitizes cortical bone to WBV,[56] WBV is expected to accelerate bone repair in OVX animals. In fact, enhanced callus formation, faster mineralization and remodeling, with the associated expression of related genes and bone markers, have been reported in WBV-treated fracture healing in OVX rats.[34,35,37] In the present bone defect model, it was observed that noise-like WBV

increased the indentation modulus of regenerated bone with no effect on its hardness and promoted increased bone regeneration (a tendency of increased Vf in the W group compared with the C group (P = 0.10)). An earlier study[57] showed a significant correlation of the indentation modulus with the mineral-to-matrix ratio, but not with either mineral maturity or collagen maturity. Thus, in contrast with iPTH, the present noise-like WBV could facilitate callus mineralization without a substantial effect on the amount of callus formation. This effect was similar between the periosteal and endosteal regions, with bone regeneration proceeding faster on the periosteal side, suggesting that the mechanical impact of noise-like WBV was independent of the degree of callus formation.

The combined treatments led to significant increases in new bone thickness and hardness, as well the amount of bone regeneration and the indentation modulus, suggesting its effectiveness for both callus formation and remodeling. Increased bone hardness, specifically in the periosteal region, has been shown to exhibit a positive correlation with mineral maturity.[57] However, interactions between iPTH and noise-like WBV were not found to be associated with structural or mechanical indices; thus, their combination should be additive and not synergistic. From the results of the individual uses of iPTH and noise-like WBV, it is likely that the principal actions of iPTH and noise-like WBV are the promotion of defect filling with immature bone and the acceleration of mineralization, respectively. However, to address the effects of noise-like WBV in combination with iPTH, evaluations at different bone healing stages are required, especially when bone healing involves both endochondral and intramembranous bone formation.

The osteogenic effect of WBV depends on vibration frequency rather than vibration magnitude or acceleration.[43,44] However, the frequency favorable for bone healing varies among studies. In fracture healing of OVX rats, WBV at a constant amplitude of 0.5 mm was more effective at 35 and 50 Hz than at 70 and 90 Hz.[36] There were also studies showing that 35-Hz and 0.3-g WBV augmented fracture healing in OVX rat bone.[34,35,37] Another study showed no effect of 0.3-g WBV at 35 Hz and a deteriorating effect

at 45 Hz in fracture healing of mice.[58] Conversely, 0.3-g WBV at 45 Hz improved fracture healing in OVX mice.[39] In these earlier studies, fracture healing occurred through a mixed process of intramembranous and endochondral bone formation, and, therefore, the increased osteogenic effects of WBV at lower frequencies would not necessarily apply to the drill-hole defect model. Indeed, 45-Hz and 0.4-g WBV enhanced bone repair in a rat calvarial defect through intramembranous ossification,[59] and 90-Hz WBV showed greater osteogenic effects in intact bone of OVX rats than WBV at lower frequencies.[43,44] To the best of our knowledge, the present study is the first to examine the osteogenic effect of noise-like WBV in bone healing. The frequency range (45–100 Hz) was arbitrarily chosen, even though reportedly-effective frequencies for osteogenic induction in OVX rodents have been previously published.[36,39,43,44] We did not explore the optimal frequency range for noise-like WBV as it was beyond the scope of this study. It would be possible that WBV using other frequency components further enhances OVX bone healing, whether WBV is used as an individual treatment or in combination with iPTH.

In addition to lacking data on the effective frequency component of noise-like WBV and using only single-time-point data, there are some limitations to be noted. Firstly, as mentioned above, in most clinical cases, bone repair occurs through a mixed process of intramembranous and endochondral bone formation. Thus, the effects of combined iPTH and noise-like WBV should be evaluated in bone repair using a more clinically-relevant animal model. Secondly, no chemical properties, such as mineral and collagen maturity, were measured. Future studies assessing the individual and combined effects of iPTH and noise-like WBV on bone components and their relationship with bone mechanical properties will provide valuable information on the effects of these treatments on bone quality. Thirdly, this study was observational and did not provide insight into the detailed mechanisms responsible for the enhanced bone healing achieved by noise-like WBV, when used separately or concurrently with iPTH. Finally, the OVX rodent models show a slow rate of cortical bone loss compared with postmenopausal patients,[60] and

unlike humans, mice lack osteons or intracortical remodeling. Thus, it is not straightforward to extrapolate the present results to fracture healing in postmenopausal patients.

Conclusions

In conclusion, 18-day treatments with iPTH and noise-like WBV for the bone defect of OVX mice accelerated intramembranous bone regeneration and increased the indentation modulus of newly formed bone, respectively. There was no interaction between iPTH and noise-like WBV in osteogenic actions, and their combination appeared to have an additive effect, leading to further regeneration of bone with high indentation modulus as well as increased hardness. These findings suggest that noise-like WBV combined with iPTH has great potential for promoting bone regeneration during osteoporotic fracture repair, in terms of both bone regeneration and mechanical function, but whether the findings could be extrapolated to fracture healing in postmenopausal women needs further study.

Declaration of Conflicting Interests

The authors declare that they have no conflict of interests related to this work.

Funding

This work was supported in part by Grants in-Aid for Scientific Research from the Ministry of Education, Culture, Sports, Science and Technology of the Japanese government (grant nos. 24650265).

References

1. Lane NE. Epidemiology, etiology, and diagnosis of osteoporosis. *Am J Obstet Gynecol* 2006; 194 Suppl 2: 3–11.
2. Yoshimura N, Muraki S, Oka H, et al. Cohort profile: research on Osteoarthritis/Osteoporosis Against Disability study. *Int J Epidemiol* 2010; 39: 988–995.
3. Yoshimura N, Muraki S, Oka H, et al. Prevalence of knee osteoarthritis, lumbar spondylosis and osteoporosis in Japanese men and women: the research on osteoarthritis/osteoporosis against dtsability study. *J Bone Miner Metab* 2009; 27: 620–628.
4. Consensus development conference: diagnosis, prophylaxis, and treatment of osteoporosis. *Am J Med* 1993; 94: 646–650.
5. He YX, Zhang G, Pan XH, et al. Impaired bone healing pattern in mice with ovariectomy-induced osteoporosis: A drill-hole defect model. *Bone* 2011; 48: 1388–1400.
6. McCann RM, Colleary G, Geddis C, et al. Effect of osteoporosis on bone mineral density and fracture repair in a rat femoral fracture model. *J Orthop Res* 2008; 26: 384–393.
7. Namkung-Matthai H, Appleyard R, Jansen J, et al. Osteoporosis influences the early period of fracture healing in a rat osteoporotic model. *Bone* 2001; 28: 80–86.
8. Oliver RA, Yu Y, Yee G, et al. Poor histological healing of a femoral fracture following 12 months of estrogen deficiency in rats. *Osteoporos Int* 2013; 24: 2581–2589.
9. Thormann U, El Khawassna T, Ray S, et al. Differences of bone healing in metaphyseal defect fractures between osteoporotic and physiological bone in rats. *Injury* 2014; 45: 487–493.
10. Walsh WR, Sherman P, Howlett CR, et al. Fracture healing in a rat osteopenia model. *Clin Orthop Relat Res* 1997; 342: 218–227.
11. Egermann M, Goldhahn J, Schneider E. Animal models for fracture treatment in osteoporosis. *Osteoporos Int* 2005; 16: S129–S138.

12. Cortet B. Bone repair in osteoporotic bone: postmenopausal and cortisone-induced osteoporosis. *Osteoporos Int* 2011; 22: 2007–2010.
13. Giannoudis P, Tzioupis C, Almalki T, et al. Fracture healing in osteoporotic fractures: is it really different? A basic science perspective. *Injury* 2007; 38 Suppl 1: 90–99.
14. Stuermer EK, Sehmisch S, Rack T, et al. Estrogen and raloxifene improve metaphyseal fracture healing in the early phase of osteoporosis. A new fracture-healing model at the tibia in rat. *Langenbecks Arch Surg* 2010; 395: 163–172.
15. Tarantino U, Cerocchi I, Celi M, et al. Pharmacological agents and bone healing. *Clin Cases Miner Bone Metab* 2009; 6: 144–148.
16. Wang JW, Xu SW, Yang DS, et al. Locally applied simvastatin promotes fracture healing in ovariectomized rat. *Osteoporos Int* 2007; 18: 1641–1650.
17. Ellegaard M, Jørgensen NR and Schwarz P. Parathyroid hormone and bone healing. *Calcif Tissue Int* 2010; 87: 1–13.
18. Jahng JS and Kim HW. Effect of intermittent administration of parathyroid hormone on fracture healing in ovariectomized rats. *Orthopedics* 2000; 23: 1089–1094.
19. Komrakova M, Stuermer EK, Werner C, et al. Effect of human parathyroid hormone hPTH (1–34) applied at different regimes on fracture healing and muscle in ovariectomized and healthy rats. *Bone* 2010; 47: 480-492.
20. Nozaka K, Miyakoshi N, Kasukawa Y, et al. Intermittent administration of human para-thyroid hormone enhances bone formation and union at the site of cancellous bone osteotomy in normal and ovariectomized rats. *Bone* 2008; 42: 90–97.
21. Aspenberg P, Genant HK, Johansson T, et al. Teriparatide for acceleration of fracture repair in humans: a prospective, randomized, double-blind study of 102 postmenopausal women with distal radial fractures. *J Bone Miner Res* 2010; 25: 404–414.

22. Peichl P, Holzer LA, Maier R, et al. Parathyroid hormone 1–8 accelerates fracture-healing in pubic bones of elderly osteoporotic women. *J Bone Joint Surg Am* 2011; 93: 1583–1587.
23. Chow JW, Fox S, Jagger CJ, et al. Role for parathyroid hormone in mechanical responsiveness of rat bone. *Am J Physiol* 1998 ;274: E146–E154.
24. Hagino H, Okano T, Akhter MP, et al. Effect of parathyroid hormone on cortical bone response to in vivo external loading of the rat tibia. *J Bone Miner Metab* 2001; 19: 244–250.
25. Kim CH, Takai E, Zhou H, et al. Trabecular bone response to mechanical and parathyroid hormone stimulation: The role of mechanical microenvironment. *J Bone Miner Res* 2003; 18: 2116–2125.
26. Li J, Duncan RL, Burr DB, et al. Parathyroid hormone enhances mechanically induced bone formation, possibly involving L-type voltage-sensitive calcium channels. *Endocrinology* 2003; 144: 1226–1233.
27. Roberts MD, Santner TJ and Hart RT. Local bone formation due to combined mechanical loading and intermittent hPTH- 1–34] treatment and its correlation to mechanical signal distributions. *J Biomech* 2009; 42: 24–38.
28. Sugiyama T, Saxon LK, Zaman G, et al. Mechanical loading enhances the anabolic effects of intermittent parathyroid hormone (1–34) on trabecular and cortical bone in mice. *Bone* 2008; 43: 238–248.
29. Tanaka S, Sakai A, Tanaka M, et al. Skeletal unloading alleviates the anabolic action of intermittent PTH (1–34) in mouse tibia in association with inhibition of PTH-induced increase in c-fos mRNA in bone marrow cells. *J Bone Miner Res* 2004; 19: 1813–1820.
30. Turner RT, Lotinun S, Hefferan TE, et al. Disuse in adult male rats attenuates the bone anabolic response to a therapeutic dose of parathyroid hormone. *J Appl Physiol* 2006; 101: 881–886.
31. Gardner MJ, van der Meulen MC, Carson J, et al. Role of parathyroid hormone in the mechanosensitivity of fracture healing. *J Orthop Res* 2007; 25: 1474–1480.

32. Prisby RD, Lafage-Proust MH, Malaval L, et al. Effects of whole body vibration on the skeleton and other organ systems in man and animal models: what we know and what we need to know. *Ageing Res Rev* 2008; 7: 319–329.
33. Slatkovska L, Alibhai SM, Beyene J, et al. Effect of whole-body vibration on BMD: a systematic review and meta-analysis. *Osteoporos Int* 2010; 21: 1969–1980.
34. Chow DH, Leung KS, Qin L, et al. Low-magnitude high-frequency vibration (LMHFV) enhances bone remodeling in osteoporotic rat femoral fracture healing. *J Orthop Res* 2011; 29: 746–752.
35. Chung SL, Leung KS and Cheung WH. Low-magnitude high-frequency vibration enhances gene expression related to callus formation, mineralization and remodeling during osteoporotic fracture healing in rats. *J Orthop Res* 2014; 32: 1572–1579.
36. Komrakova M, Sehmisch S, Tezval M, et al. Identification of a vibration regime favorable for bone healing and muscle in estrogen-deficient rats. *Calcif Tissue Int* 2013; 92: 509–520.
37. Shi HF, Cheung WH, Qin L, et al. Low-magnitude high-frequency vibration treatment augments fracture healing in ovariectomy-induced osteoporotic bone. *Bone* 2010; 46: 1299–1305.
38. Stuermer EK, Komrakova M, Werner C, et al. Musculoskeletal response to whole-body vibration during fracture healing in intact and ovariectomized rats. *Calcif Tissue Int* 2010 ;87: 168–180.
39. Wehrle E, Liedert A, Heilmann A, et al. The impact of low-magnitude high-frequency vibration on fracture healing is profoundly influenced by the oestrogen status in mice. *Dis Model Mech* 2015; 8: 93–104.
40. Robling G and Turner CH. Mechanotransduction in bone: genetic effects on mechanosensitivity in mice. Bone 2002; 31: 562–569.
41. Judex S, Donahue LR and Rubin C. Genetic predisposition to low bone mass is paralleled by an enhanced sensitivity to signals anabolic to the skeleton. FASEB J 2002; 16: 1280–1282.
42. Warden SJ, Komatsu DE, Rydberg J, et al. Recombinant human parathyroid hormone (PTH 1–34) and

low-intensity pulsed ultrasound have contrasting additive effects during fracture healing. *Bone* 2009; 44: 485–494.

43. Judex S, Lei X, Han D, et al. Low-magnitude mechanical signals that stimulate bone formation in the ovariectomized rat are dependent on the applied frequency but not on the strain magnitude. *J Biomech* 2007; 40: 1333–1339.
44. Pasqualini M, Lavet C, Elbadaoui M, et al. Skeletal site-specific effects of whole body vibration in mature rats: from deleterious to beneficial frequency-dependent effects. *Bone* 2013; 55: 69–77.
45. Otsu N. Threshold selection method from gray-level histograms. *IEEE Trans Syst Man Cybern* 1979; 9: 62–66.
46. Doube M, Kłosowski MM, Arganda-Carreras I, et al. BoneJ: free and extensible bone image analysis in ImageJ. *Bone* 2010; 47: 1076–1079.
47. Hengsberger S, Kulik A and Zysset P. Nanoindentation discriminates the elastic properties of individual human bone lamellae under dry and physiological conditions. *Bone* 2002; 30: 178–184.
48. Matsumoto T, Miyakawa T and Yamamoto D. Effects of vitamin K on the morphometric and material properties of bone in the tibiae of growing rats. *Metabolism* 2012; 61: 407–414.
49. Oliver WC and Pharr GM. Measurement of hardness and elastic modulus by instrumented indentation: Advances in understanding and refinements to methodology. *J Mater Res* 2004; 19: 3–20.
50. Monfoulet L, Rabier B, Chassande O, et al. Drilled hole defects in mouse femur as models of intramembranous cortical and cancellous bone regeneration. *Calcif Tissue Int* 2010; 86: 72–81.
51. Thompson Z, Miclau T, Hu D, et al. A model for intramembranous ossification during fracture healing. *J Orthop Res* 2002; 20: 1091–1098.
52. Jerome CP, Burr DB, Van Bibber T, et al. Treatment with human parathyroid hormone (1–34) for 18 months increases cancellous bone volume and improves trabecular architecture in ovariectomized cynomolgus monkeys (Macaca fascicularis). *Bone* 2001; 28: 15–19.

53. Sato M, Westmore M, Ma YL, et al. Teriparatide [PTH(1–34)] strengthens the proximal femur of ovariectomized nonhuman primates despite increasing porosity. *J Bone Miner Res* 2004; 19: 623–629.
54. Wronski TJ, Yen CF, Qi H, et al. Parathyroid hormone is more effective than estrogen or bisphosphonates for restoration of lost bone mass in ovariectomized rats. *Endocrinology* 1993; 132: 823–831.
55. Komatsu DE, Brune KA, Liu H, et al. Longitudinal in vivo analysis of the region-specific efficacy of parathyroid hormone in a rat cortical defect model. *Endocrinology* 2009; 150: 1570–1579.
56. Rubinacci A, Marenzana M, Cavani F, et al. Ovariectomy sensitizes rat cortical bone to whole-body vibration. *Calcif Tissue Int* 2008; 82: 316–326.
57. Busa B, Miller LM, Rubin CT, et al. Rapid establishment of chemical and mechanical properties during lamellar bone formation. *Calcif Tissue Int* 2005; 77: 386–394.
58. Wehrle E, Wehner T, Heilmann A, et al. Distinct frequency dependent effects of whole-body vibration on non-fractured bone and fracture healing in mice. *J Orthop Res* 2014; 32: 1006–1013.
59. Hwang SJ, Lublinsky S, Seo YK, et al. Extremely small-magnitude accelerations enhance bone regeneration: a preliminary study. *Clin Orthop Relat Res* 2009; 467: 1083–1091.
60. Kimmel DB and Wronski TJ. Nondestructive measurement of bone mineral in femurs from ovariectomized rats. Calcif Tissue Int 1990; 46: 101–110.

Table 1　Structural indexes of regenerated bone

	C	P	W	PW
Vf [%]	37.2±13.7	57.4±13.5*	52.2±18.2	64.3±16.9***
Th [μm]	69.2±19.8	90.7±23.2	82.9±14.0	93.6±24.3*
Seg.N [/mm^3]	8473±2660	10210±2841	9723±5113	9580±2846
Seg.C [/mm^3]	522±333	487±164	425±180	441±210

C: control mice, P: mice treated with iPTH, W: mice treated with noise-like WBV, PW: mice treated with both iPTH and noise-like WBV.
Vf, fraction of volume; Th, mean thickness; Seg.N, segment number; Seg.C, connectivity density.
$^{*}P<0.05$, $^{***}P<0.001$ vs. C.

Figure captions

Figure 1. (A) Whole-body vibration (WBV) system for mice. The compartmented cage attached to a vibration platform is moved by an electromagnetic actuator. The platform vibration is monitored by an accelerometer and a laser displacement sensor. (B) Example graphs of acceleration and displacement, and power spectral density (PSD) of acceleration are shown. The system operates to generate a Gaussian quasi-white noise-like vibration with frequency components of 45–100 Hz and a root mean squared acceleration of 0.3 g.

Figure 2. Radiographs of drill-holed tibia and its defect segment on the frontal and lateral sides from a control mouse. The intercortical circle and square indicate the cylindrical region for analysis. Bar: 250 μm.

Figure 3. (A) Cortical bone specimen embedded in polymethylmethacrylate and defect regions segmented for the nanoindentation test. (B) An example of force–displacement curve, produced by nanoindentation testing using a loading-holding-unloading profile.

Figure 4. Three-dimensional isosurface displays of regenerated bone in control (C), intermittent parathyroid hormone (iPTH)-treated (P), WBV-treated (W), and iPTH and WBV-treated (PW) groups, viewed from the periosteal and endosteal sides. The lengths of the orthogonal thick line segments are all 100 μm.

Figure 5. Effect of iPTH and WBV on the stiffness and hardness of regenerated bone. There were no significant iPTH×WBV interactions in both indexes, as determined by two-way ANOVA. C: control mice, P: mice treated with iPTH, W: mice treated with noise-like WBV, PW: mice

treated with both iPTH and noise-like WBV. $^{*}P<0.05$, $^{**}P<0.01$ vs. C; $^{\#}P<0.01$ vs. periosteal region.

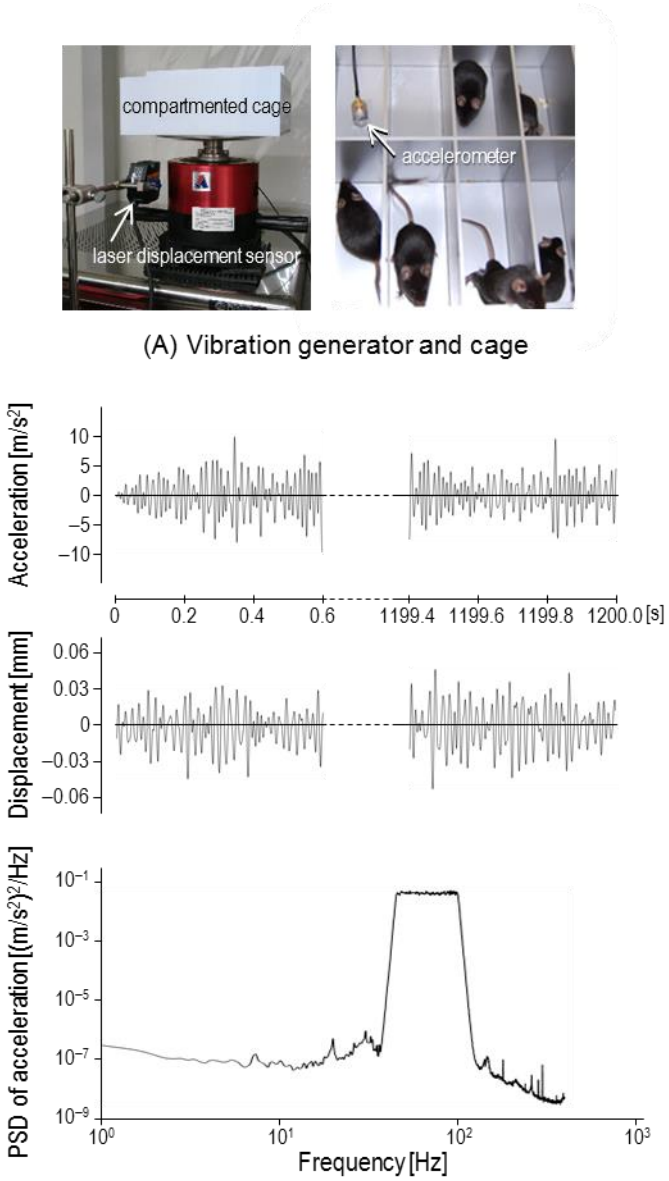
compartmented cage
laser displacement sensor
accelerometer
(A) Vibration generator and cage
Acceleration [m/s²]
10
5
0
−5
−10
0
0.2
0.4
0.6
1199.4
1199.6
1199.8
1200.0 [s]
Displacement [mm]
0.06
0.03
0
−0.03
−0.06
PSD of acceleration [(m/s²)²/Hz]
10⁻¹
10⁻³
10⁻⁵
10⁻⁷
10⁻⁹
10⁰
10¹
10²
10³
Frequency [Hz]
(B) Noise-like WBV (Gaussian quasi-white noise)

Figure 1

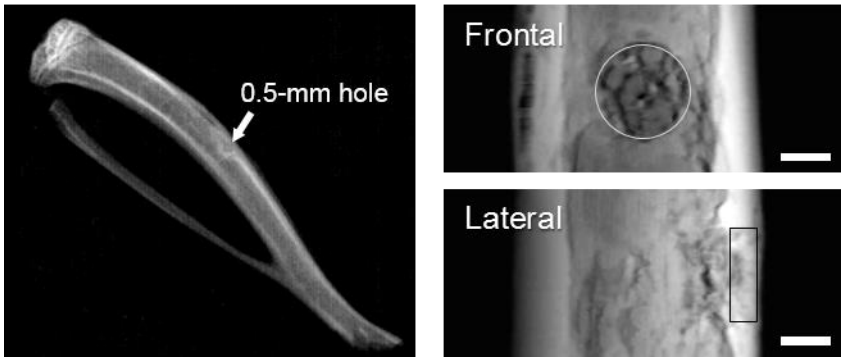

Figure 2

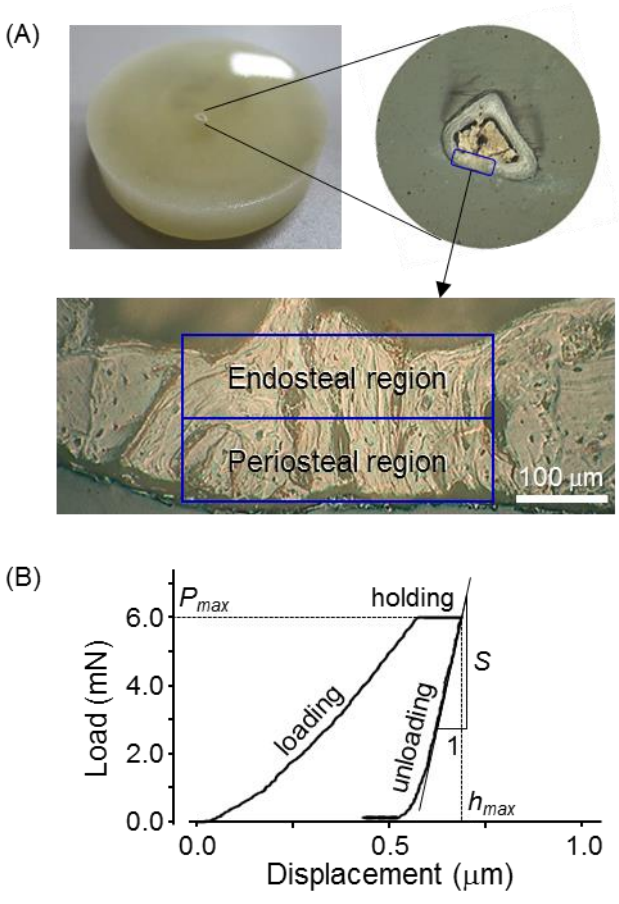
(A)
Endosteal region
Periosteal region
100 μm
(B)
P_{max}
holding
6.0
4.0
2.0
0.0
Load (mN)
loading
unloading
S
1
h_{max}
0.0
0.5
1.0
Displacement (μm)

Figure 3

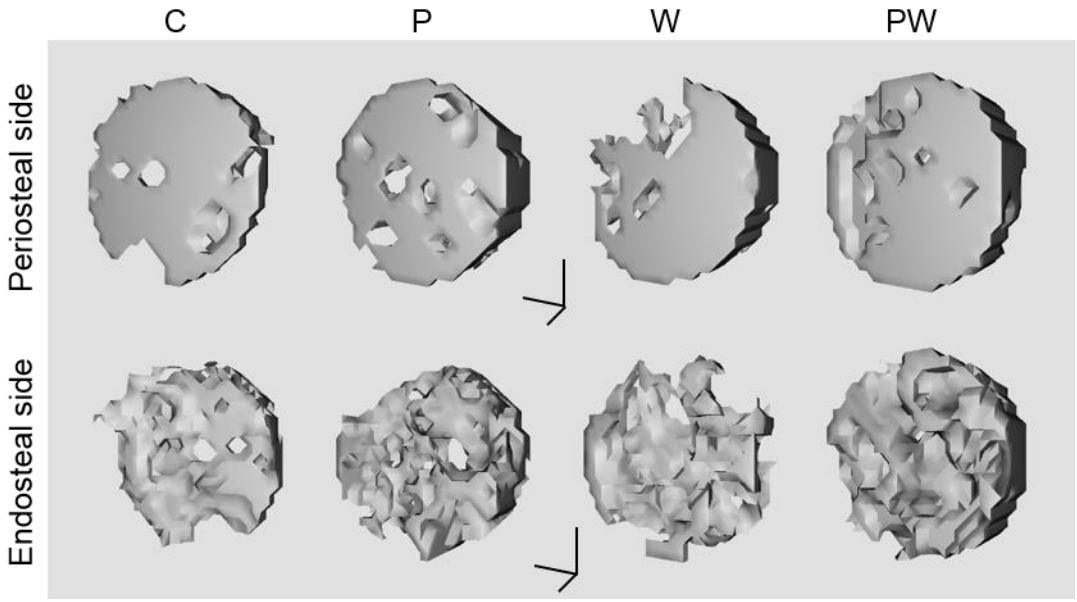

Figure 4

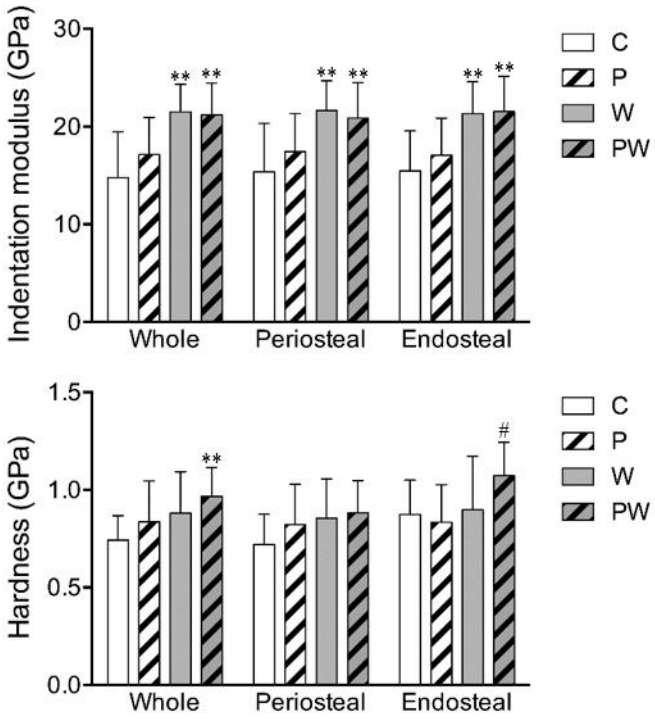
Indentation modulus (GPa)
30
20
10
0
**
**
**
**
**
**
Whole
Periosteal
Endosteal
C
P
W
PW
Hardness (GPa)
1.5
1.0
0.5
0.0
**
#
Whole
Periosteal
Endosteal
C
P
W
PW

Figure 5